Electronic Supplementary Material (ESI) for Physical Chemistry Chemical Physics.

Supporting Information

Influence of the donor unit on the rectification ratio in tunnel junctions based on donor-acceptor SAMs

Manuel Souto,[a]† Valentin Díez-Cabanes,[b] Li Yuan,[c]‡ Adriana Kyvik,[a] Imma Ratera,[a] Christian A. Nijhuis,*[cde] Jerome Cornil*[b] and Jaume Veciana*[a]

Contents

1. General methods for synthesis and characterization

All reagents and solvents employed for the syntheses were of high purity grade and were purchased from Sigma-Aldrich Co., Merck, and SDS. Dry solvents were used in the chemical reactions and in the cyclic voltammetries. Chlorinated solvents were filtered with basic alumina in order to deactivate the acidic points. ^{1}H NMR spectra were recorded using a Bruker Avance 250, 400, or 500 instruments and Me_4Si as an internal standard. Infrared spectra were recorded with Spectrum One FT-IR Spectroscopy instrument and UV/Vis/NIR spectra were measured using Cary 5000E Varian. ESR spectra were performed with a Bruker ESP 300 E equipped with a rectangular cavity T102 that works with an X-band (9.5 GHz). The solutions were degassed by argon bubbling before the measurements. LDI/TOF MS were recorded in a Bruker Ultraflex LDI-TOF spectrometer. Cyclic voltammetry measurements were obtained with a potentiostat 263a from EG&G Princeton Applied Research in a standard 3 electrodes cell. The IR-NIR spectra have been collected with a Bruker FT-IR IFS-66 spectrometer equipped with a Hyperion microscope. The spectral resolution is about 2 cm^{-1} for both spectrometers. TOF-SIMs measurements of SAMs were recorded using a primary gun that was bombardment with Bi ions with the following intensities: 1.2 pA (Bi^+), 0.3 pA ($Bi^{+\,3}$, 0.2 pA ($Bi^{++\,3}$).

2. Synthesis and characterization of PTM-TTF based dyads 3 and 4

Synthesis of 5

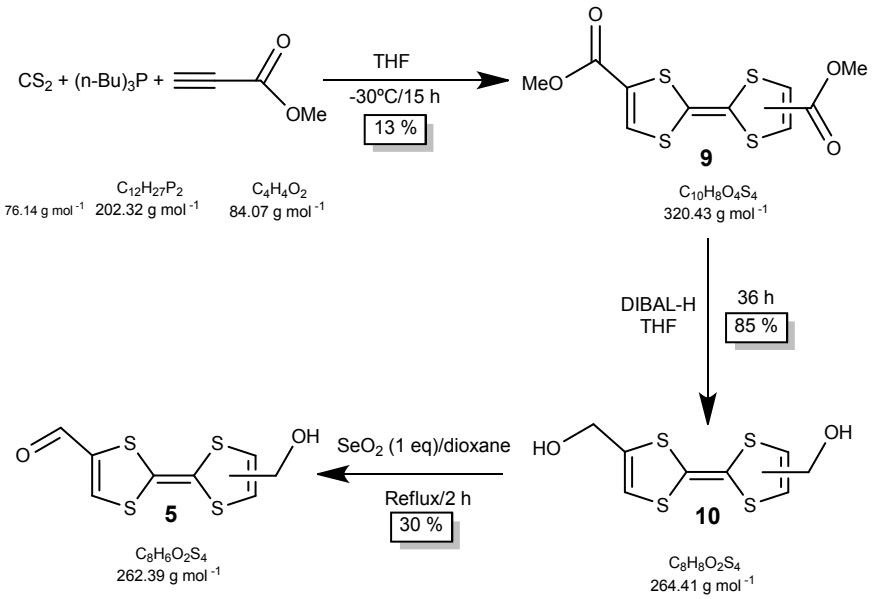

Synthesis of 9

Tributylphosphine (20.3 g, 0.1 mol) was added dropwise to a solution of 10 mL of carbon disulfide in 50 mL of tetrahydrofuran at -10ºC under inert conditions and the deep maroon solution was stirred at room temperature for 1 hour. Next the mixture was cooled to -40ºC and a solution of methyl propiolate (8.4 g, 0.1 mol) in 20 mL of tetrahydrofuran was added dropwise. The temperature was maintained between -30ºC and -50ºC during the addition. The solution was warmed to room temperature and stirred overnight. Finally solvents were evaporated under reduced pressure, the residue was stirred with ether to crash out the product that and was filtered and washed with Et_2O to give 4.2 g (13 %) of the red microcrystalline powder **9**. **Characterization**: **^{1}H-NMR** (250 MHz, $CDCl_3$, δ(ppm): 7.35 (d, 2H, CH, J = 7.34 Hz); 3.82 (s, 6H, CH_3). **FT-IR** (ν cm^{-1}): 2956 (w); 2922 (w); 2852 (w); 1712 (s, C=O); 1548 (s); 1434 (m); 1244 (s); 1199 (m); 1045 (m); 940 (m); 829 (m); 820 (m); 763 (m); 725 (m). **LDI-TOF** (positive mode): *m/z* (amu/e^-): 320.377 ($M^{+\cdot}$).

Synthesis of 10

30 mL of DIBAL-H (1 M in THF) was added dropwise to a solution of 4,4'(5')-Bis(methoxycarbonyl) tetrathiafulvalene (**9**) (1 g, 3.12 mmol) in 60 ml of tetrahydrofuran cooled at -70ºC under strict inert conditions. The color of the solution changes from red to yellow during the first hour of reaction. Then the solution was allowed to warm to room temperature and stirred overnight. The absence of TTF diester was confirmed by TLC and the reaction was hydrolyzed by the carefully addition of 10 mL of MeOH/HCl 12 M (3:1) mixture to the solution previously cooled with an ice bath. Then ether was added to the mixture and the organic phase was washed with three portions of water (100 mL), dried with anhydrous $MgSO_4$ and solvents were evaporated under reduced pressure. Finally the product was purified by column chromatography of silica gel using a mixture of ether and hexane to obtain 738 mg (85 %) of TTF diol **10** as a light brown solid. **Characterization**: **^{1}H-NMR** (250 MHz, DMSO-D_6, δ(ppm): 6.52 (s, 2H, CH); 5.48 (t, 2H, J = 5.9 Hz, OH); 4.20 (d, 4H, J = 5.84 Hz, **CH_2**OH). **FT-IR** (ν cm^{-1}): 3338 (s, OH); 3256 (s, OH); 2947 (m); 2918 (m); 2858 (m); 1587 (w); 1459 (m); 1443 (m); 1430 (m); 1369 (m); 1228 (m); 1092 (s); 1012 (s); 969 (m); 839 (w); 773 (w); 741 (w) 709 (w). **LDI-TOF** (positive mode): *m/z* (amu/e$^-$): 263.926 ($M^{+\cdot}$).

Synthesis of 5

A solution of equimolar amounts of 2,6(7)-bis(hydroxymethyl)-TTF (**10**) (750 mg, 2.84 mmol) and selenium dioxide (315 mg) was heated under reflux for 2 h in dry dioxane (70 mL); the solution turned from yellow to dark red. Cooling of the solution resulted in the formation of a black precipitate of elemental selenium, which was filtered and washed thoroughly with dichloromethane. The solvent mixture was then evaporated under reduced pressure to produce a dark red oil, which was purified by SiO_2 column chromatography (eluent: hexane: Et_2O) to afford a fraction that corresponds to the 2-formyl- 6(7)-hydroxymethyl TTF (**5**) (220 mg, 30%) as a violet microcrystalline powder. **Characterization**: **^{1}H-NMR** (250 MHz, DMSO-D_6, δ(ppm): 9.53 (s, 1H, CHO); 8.26 (s, 1H); 6.60 (s, 1H); 5.55 (t, J = 5.2 Hz, 1H, OH); 4.23 (d, 2H, J = 5.2 Hz, CH_2OH). **FT-IR** (ν cm^{-1}): 3405 (m, OH); 2918 (m); 2851 (m); 1721 (w); 1625 (s, C=O); 1540 (m); 1512 (s); 1363 (m); 1280 (w); 1230 (m); 1140 (s); 1109 (m); 1010 (m); 954 (m); 839 (s); 747 (m). **LDI-TOF** (positive mode): *m/z* (amu/e$^-$): 261.976 ($M^{+\cdot}$).

Synthesis of 7

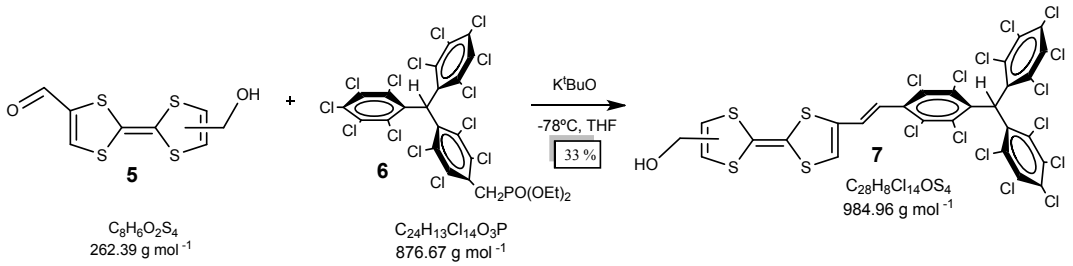

600 mg (0.68 mmol) of the phosphonated PTM derivative (**6**)[1] were dissolved in 50 mL of anhydrous THF under strict inert conditions. The solution was cooled down to -78 ºC. Next, 130 mg (1.15 mmol) of potassium *tert*-butoxide were added and stirred for 20 minutes to form the yellow-orange ylide. Then 195 mg (0.75 mmol) of 2-formyl-6(7)-hydroxymethyl tetrathiafulvalene (**5**) were added and the reaction was warmed up to room temperature and stirred for 2 days. Then the mixture was washed with water, dried with anhydrous $MgSO_4$ and solvents were evaporated under reduced pressure. Finally the product was purified by column chromatography of silica gel using a mixture of ether and hexane to obtain to obtain 220 mg (33 %) of hydroxymethyl-TTF-PTMαH (**7**) as a red powder. **Characterization**: **^{1}H-NMR** (250 MHz, DMSO-D_6, δ(ppm): 7.18 (s, 1H, αH); 7,14 (d, J = 16.1 Hz, 1H, CH=CH); 6.91 (s, 1H, C**H**=C-CH=CH); 6.58 (s, 1H, C**H**=C-CH_2OH); 6.31 (d, J = 16.2 Hz, CH=CH); 5.33 (t, J = 5.53 Hz, 1H, OH); 4.23 (d, J = 4.7 Hz, 2H, C**H_2**OH). **FT-IR** (ν cm^{-1}): 3368 (m, OH); 2956 (m); 2922 (m); 2855 (m); 1614 (m, CH=CH); 1517 (m); 1454 (m); 1357 (s); 1337 (s); 1296 (s); 1188 (w); 1139 (m); 1116 (m); 1019 (m); 941 (m); 862 (w);

808 (s); 776 (m) 750 (s); 713 (m); 682 (m). **LDI-TOF** (positive mode): *m/z* (amu/e$^-$): 983.515 ($M^{+\cdot}$). **Cyclic voltammetry** (Bu_4NPF_6 0.15 M in CH_2Cl_2 as electrolyte): $E_{½}^1$ = 0.47 V; $E_{½}^2$ = 0.97 V.

Synthesis of PTM-TTF based dyad 3

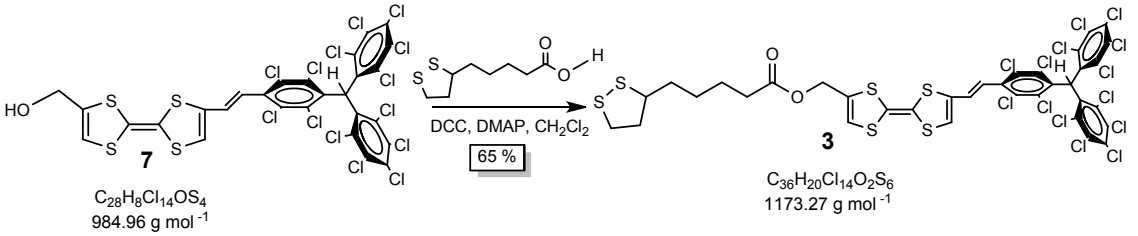

60 mg (0.04 mmol) of **7** and 15 mg thioctic acid (1.2 molar equiv.) were dissolved in 15 mL of distilled CH_2Cl_2 and stirred at 0 °C (ice/water bath) under Ar for 15 min. Then 20 mg (1.5 molar equiv.) of 1,3-dicyclohexylcarbodiimide (DCC) and 2.3 mg (0.3 molar equiv.) of 4-(dimethylamino)-pyridine (DMAP) were added to the solution and the mixture was stirred for another 15 min at 0 °C. The cooling bath was then removed, and the solution was allowed to warm at room temperature overnight. Next the reaction mixture was washed with water (50 mL) and the organic layer was dried over $MgSO_4$, filtered, and evaporated. The residue was purified by column chromatography (CH_2Cl_2/Hexane) and precipitated with methanol to obtain 46 mg of **3** (65 %) as a red powder. **Characterization**: **^{1}H-NMR** (250 MHz C_6D_6, δ (ppm): 7.21 (s, 1H, αH); 6,29 (d, J = 16.1 Hz, 2H, CH=CH); 6.14 (d, J = 16.1 Hz, 2H, CH=CH); 5.52 (s, 1H, TTF); 5.46 (s, 1H, TTF); 4.42 (s, 2H, COO-CH_2-TTF); 3.92-3.78 (m, 1H); 3.61-3.52 (m, 1H); 3.19-3.06 (m, 1H); 2.70-2.54 (m, 2H); 1.97 (td, 7.2, 4.0 Hz, 3H); 1.88-1.74 (m, 3 H); 1.60-1.49 (m, 2H). **FT-IR** (ν cm^{-1}): 2952 (m); 2922 (s); 2851 (s); 1738 (s, C=O); 1614 (m, C=C); 1517 (m); 1456 (m); 1370 (m); 1335 (m); 1296 (m); 1235 (w); 1136 (m); 1020 (w); 943 (m); 862 (w); 808 (s); 774 (m); 754 (m); 696 (w) 683 (w). **UV-VIS-NIR** (CH_2Cl_2, λ_{max} in nm, ε in $M^{-1}\cdot cm^{-1}$): 231 (62565); 305 (22253); 449 (3942). **LDI-TOF** (positive mode): *m/z* (amu/e$^-$): 1171.39 ($M^{+\cdot}$). **Cyclic voltammetry** (Bu_4NPF_6 0.15 M in CH_2Cl_2 as electrolyte): $E_{½}^1$ = 0.435 V; $E_{½}^2$ = 0.891 V; $E_{½}^3$ = 1.08 (S-S).

Synthesis of PTM-TTF based dyad 4

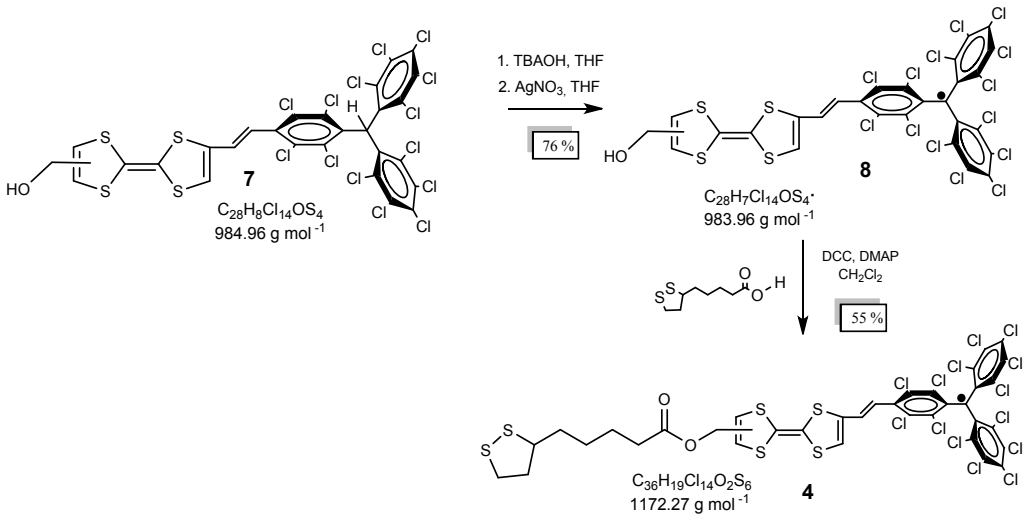

Synthesis of 8

50 mg (0.05 mmol) of **7** were dissolved in 20 mL of dry THF and 100 μL (0.1 mmol) of tetrabutylammonium hydroxide 1.0 M in water were added and the purple solution was stirred for 40 minutes. Then the reaction mixture was stirred with 17 mg (0.1 mmol) of silver nitrate in THF/AcMe (5:1) for 20 minutes. The solution changes from purple to dark brown with silver (Ag^0) precipitated. Then the solution was filtered and the solvent was evaporated under reduced pressure. Finally, the product was purified by flash column chromatography of silica gel using CH_2Cl_2 as eluent and precipitated with methanol to produce 38 mg of radical **6** (76 %). **Characterization**: **FT-IR** (ν cm^{-1}): 3405 (m, OH); 2955 (m); 2922 (m); 2855 (m); 1728 (w); 1604 (m, CH=CH); 1506 (m); 1460 (m); 1335 (s); 1261 (s); 1160 (w); 1137 (w); 1118 (w); 1029 (m); 940 (m); 865 (w); 817 (m); 774 (w) 754 (w); 735 (m); 709 (m); 696 (w); 680 (w). **UV-VIS-NIR** (CH_2Cl_2, λ_{max} in nm, ε in $M^{-1}\cdot cm^{-1}$): 296 (18087); 319 (16067); 387 (20004); 425 (11174). **LDI-TOF** (positive mode): *m/z* (amu/e^-): 982.793 ($M^{+\cdot}$); (negative mode): 982.796 ($M^{-\cdot}$). **Cyclic voltammetry** (Bu_4NPF_6 0.15 M in CH_2Cl_2 as electrolyte):$E_{½}^1$ = -0.188 V; $E_{½}^2$ = 0.476 V; $E_{½}^3$ = 0.956 V.

Synthesis of dyad 4

40 mg (0.04 mmol) of **8** and 10 mg thioctic acid (1.2 molar equiv.) were dissolved in 10 mL of distilled CH_2Cl_2 and stirred at 0 °C (ice/water bath) under Ar for 15 min. Then 13 mg (1.5 molar equiv.) of 1,3-dicyclohexylcarbodiimide (DCC) and 1.5 mg (0.3 molar equiv) of 4-(dimethylamino)-pyridine (DMAP) were added to the solution and the mixture was stirred for another 15 min at 0 °C. The cooling bath was then removed, and the solution was allowed to warm at room temperature overnight. Next the reaction mixture was washed with water (50 mL) and the organic layer was dried over $MgSO_4$, filtered, and evaporated. The residue was subjected to column chromatography (CH_2Cl_2/Hexane) and precipitated with methanol to obtain 26 mg of radical dyad **4** (55 %). **Characterization**: **FT-IR** (ν cm^{-1}): 2955 (m); 2922 (s); 2855 (s); 1736 (m, C=O); 1662 (w); 1604 (w, C=C); 1554 (w); 1499 (w); 1460 (m); 1372 (w); 1335 (s); 1259 (m); 1159 (w); 1135 (w); 1120 (w); 1028 (w); 940 (m); 865 (w); 817 (m); 776 (w); 735 (w); 708 (w); 693 (w).). **UV-VIS-NIR** (CH_2Cl_2, λ_{max} in nm, ε in $M^{-1}\cdot cm^{-1}$): 293 (16515); 324 (15110); 387 (16555); 425 (9368). L**DI-TOF** (negative mode): *m/z* (amu/e^-): 1171.638 ($M^{-\cdot}$). L**DI-TOF** (positive mode): *m/z* (amu/e^-): 1172.794 ($M^{+\cdot}$); (negative mode): 1172.878 ($M^{-\cdot}$). **Cyclic voltammetry** (Bu_4NPF_6 0.15 M in CH_2Cl_2 as electrolyte):$E_{½}^1$ = -0.239 V; $E_{½}^2$ = 0.477 V; $E_{½}^3$ = 0.861 V.

^{1}H-NMR of 7

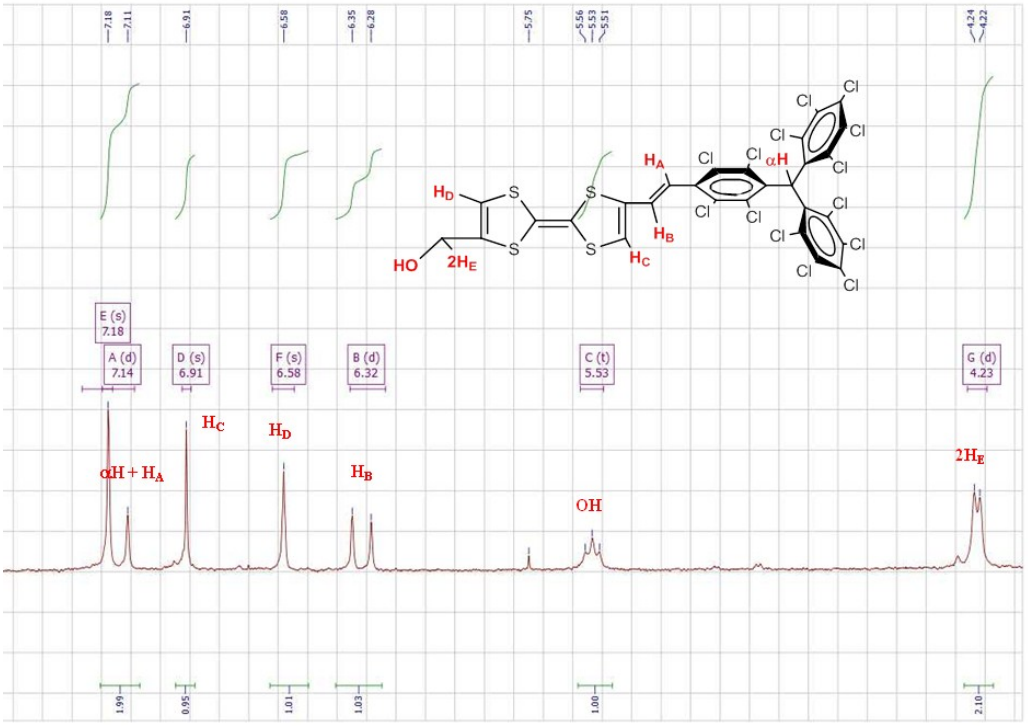

Figure S1. ^{1}H-NMR spectrum of compound **7** in DMSO-D_6 and protons observed in the ^{1}H-NMR spectrum.

^{1}H-NMR of PTM-TTF based dyad 3

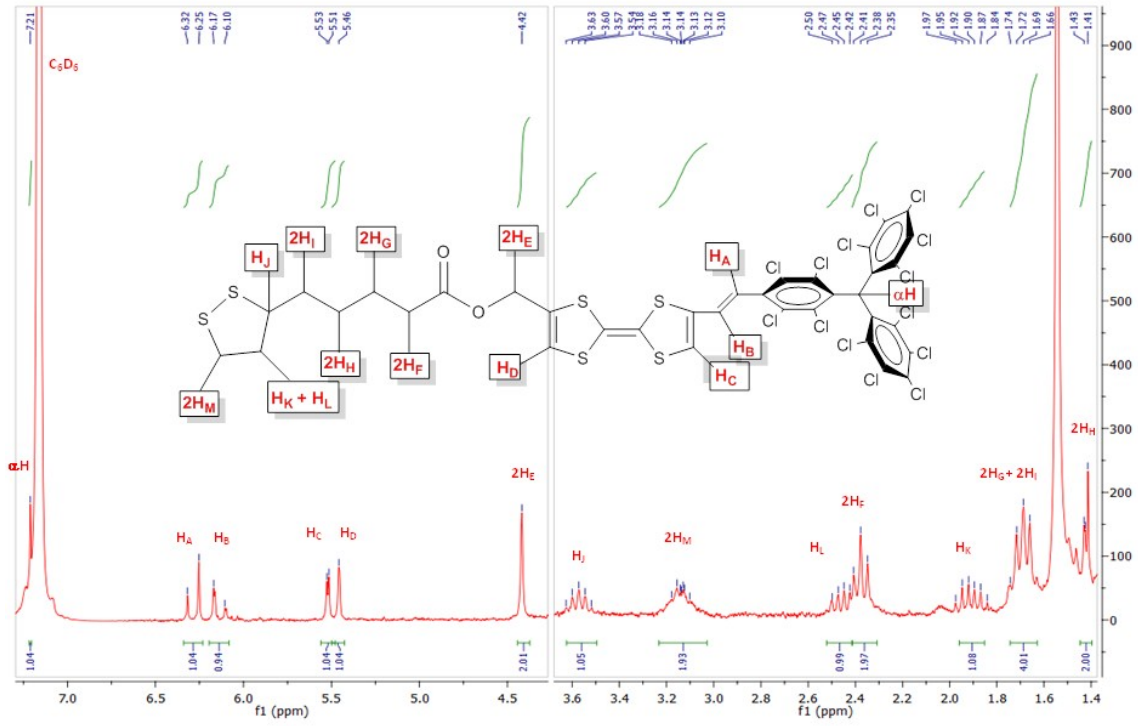

Figure S2. ^{1}H-NMR spectrum of compound **3** in C_6D_6 and protons observed in the ^{1}H-NMR spectrum.

UV-vis-NIR of PTM-TTF based dyads 3 and 4

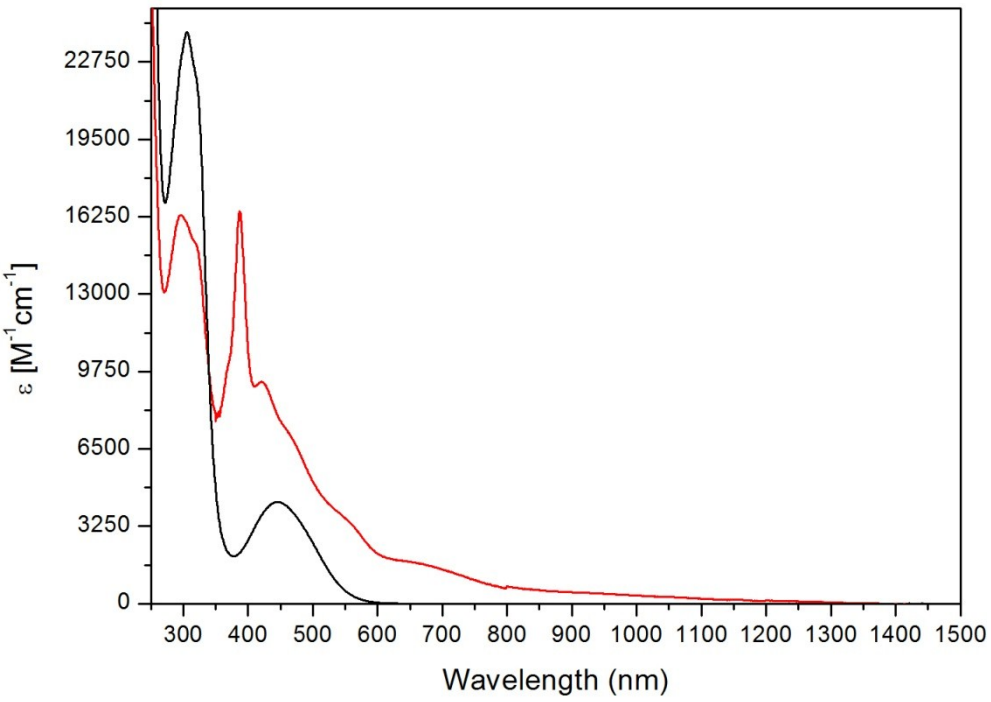

Figure S3. UV-Vis-NIR spectra of a solution 0.05 mM of nonradical disulfide derivative **3** (black line) and radical disulfide derivative **4** (red line) in CH_2Cl_2 at room temperature.

IR of PTM-TTF based dyads 3 and 4

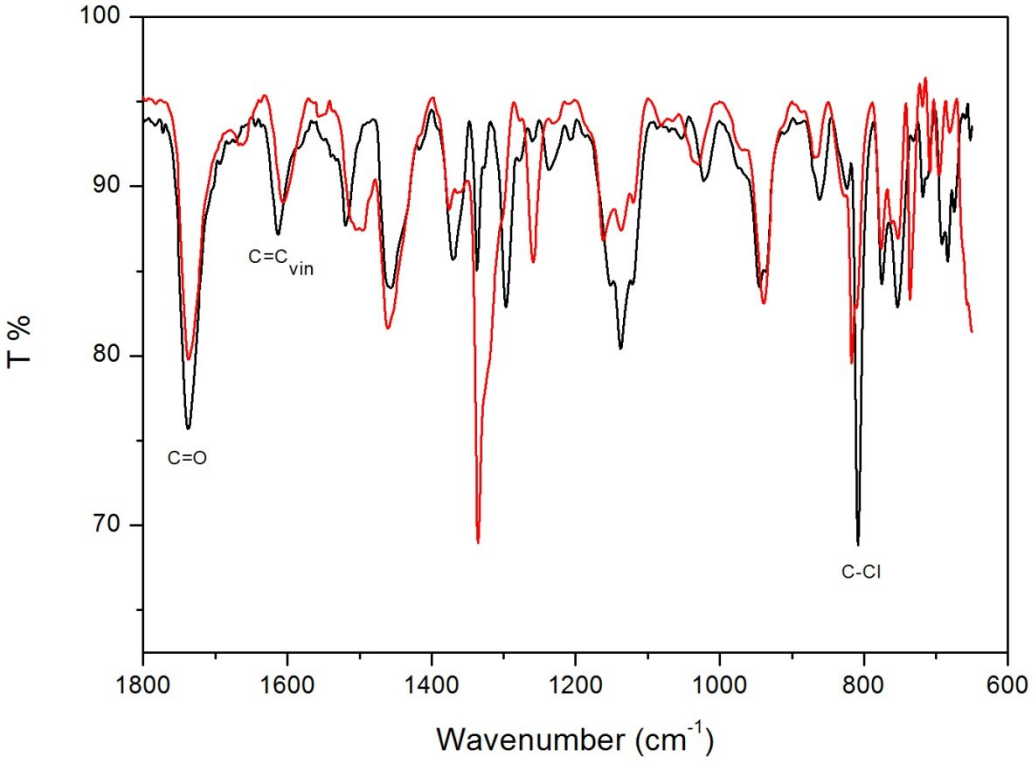

Figure S4. FT-IR spectra of nonradical disulfide derivative **3** (black line) and radical disulfide derivative **4** (black line) in the 1800-600 cm^{-1} region**.**

CV of PTM-TTF based dyads 3 and 4

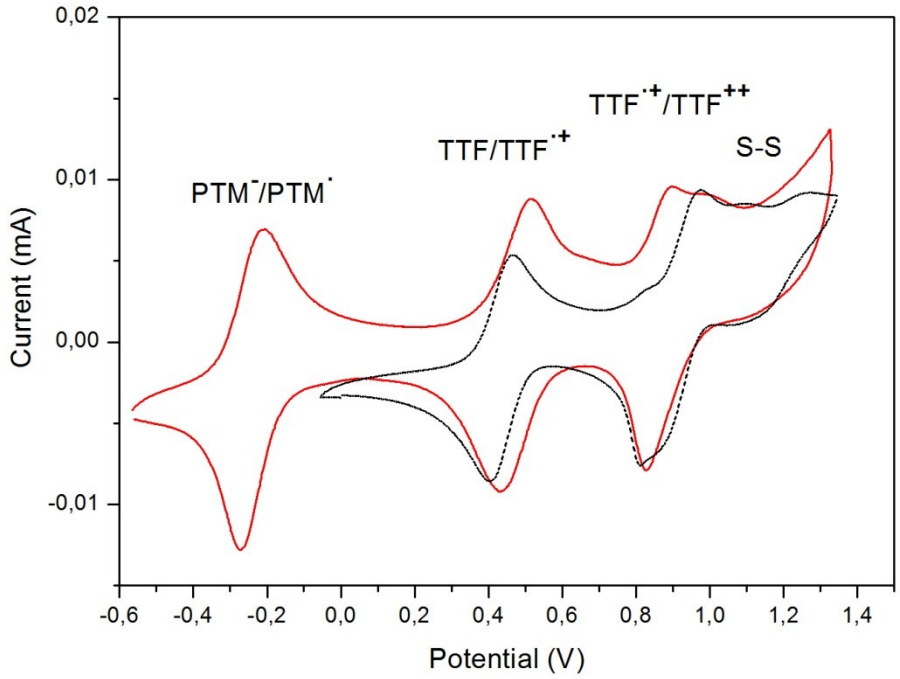

Figure S5. Cyclic voltammetries of nonradical disulfide derivative **3** (black line) and radical disulfide derivative **4** (red line) in CH_2Cl_2 vs. Ag/AgCl under Argon (*n*-Bu_4PF_6 (0.1 M) as electrolyte, 300 K, scan rate of 0.1 V/s).

3. General procedures for the device preparation and characterization

3.1. Ultraflat template surfaces

We have reported the procedure to fabricate the ultraflat Au surfaces by a template-stripping (TS) method where else.[2] Here, we only give a short description with key experimental factors as follow. We deposited 200 nm thick Au with 99.999% purity (Super Conductor Materials Inc) film on clean Si (100) wafers with their native SiO_2 surface layer by thermal deposition (Shen Yang Ke Yi, China) with a base pressure of 2×10^{-6} mbar. The deposition rate of the first 50 nm thick Au was about 0.3 Å/s and then increased to about 5 Å/s for the rest 150 nm. We used the thermal curable epoxy (EpoTek, 353ND) to glue the clean glass slides on the Au surfaces. The epoxy was cured at 80 °C for 8 hour in an oven. We only cleaved off the metal surface with glass slide as support from the Si wafer before the immersion of the Au^{TS} surfaces into the thiol solutions, in order to minimize the contamination from air.

3.2. Preparation of the PTM-TTF based SAMs 3 and 4

Au^{TS} surfaces were immersed in a freshly prepared solution of 1 mM of each compound (**1** or **2**) in toluene (HPLC grade) during the first hour at 40 °C and then for additional 24-48 hours at room temperature. Always, before immersing the substrates, the solution was degassed with argon. During the SAM formation the solution was kept in dark and under argon atmosphere to avoid the decomposition of the radical species. After the time indicated above, the substrates were removed from the solution and were washed with toluene to remove any physisorbed material. The modified substrates were characterized immediately after being removed from the solution.

3.3. ToF-SIMs of PTM-TTF based SAM 4

We performed ToF-SIMs measurements in order to demonstrate the presence and anchoring of compound **3** and **4** to the Au surface. The mass spectra obtained are shown in Figure S6 where the highest m/z fragment detected for SAMs of **4** was the one corresponding to the entire molecule (MW=1172 g/mol).

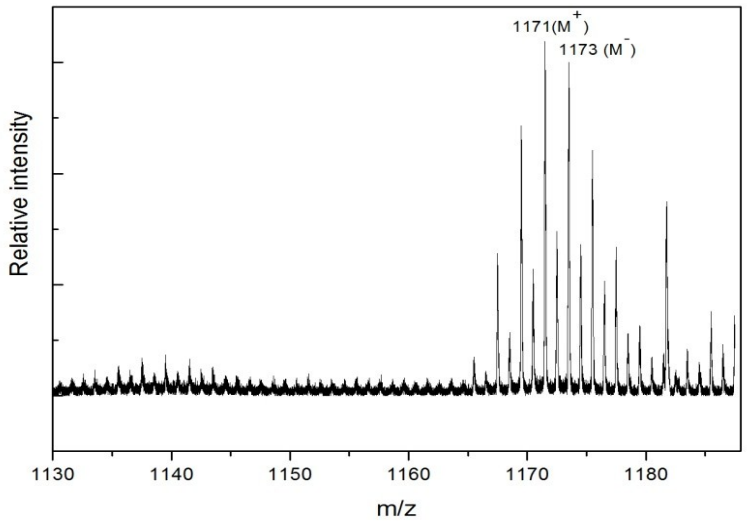

Figure S6. Positive mode ToF-SIMS mass spectrum of **SAM** derived from dyad **4**. Zoom of the specific region showing the highest m/Z fragment detected for SAMs of **4** corresponding to the entire molecule (MW=1154 g/mol).

3.4. ESR of PTM-TTF based SAM 4

The magnetic character of the radical molecules grafted on SAM **4** was also checked by ESR. Indeed, the ESR spectrum (Figure S7) showed a signal at g = 2.0032 with a linewidth (δH) of 5.2 Gauss. SAM **3** did not present any ESR signal because in this case the PTM moiety is a diamagnetic closed-shell species.

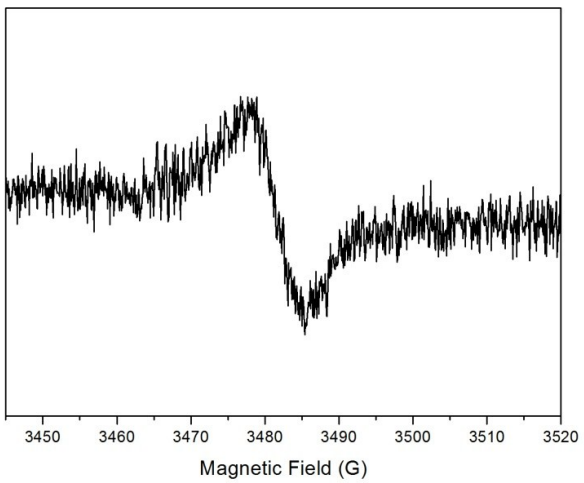

Figure S7. ESR spectra of SAM of **PTM-TTF based SAM 4**.

3.5. Electrochemical characterization of PTM-TTF based SAMs 3 and 4

The electrochemical characterization was performed using substrates of 300 nm Au evaporated on mica from Georg Albert (Germany). Before their use, the substrates were rinsed with acetone, dichloromethane, and ethanol, and then exposed to ozone for 20 minutes. Immediately after that the substrates were immersed in ethanol (HPLC grade) for at least 30 minutes. Before immersing the substrates in the PTM derivative solution, they were rinsed with ethanol and dried under nitrogen stream. The procedure followed for the formation of the SAM is the same as described for Au^{TS}. The two SAMs **3** and **4** were electrochemically characterized by using cyclic voltammetry (CV) performed with an AUTOLAB 204 with NOVA 1.9 software. We used a custom built electrochemical cell with a Pt-wire as counter electrode, Ag-wire as quasi-reference electrode and the modified Au on mica as working electrode. The area exposed to the lithium perchlorate ($LiClO_4$) in acetonitrile electrolyte solution (0.1 M) was 0.26 cm^2. The CVs were recorded in the range from -0.5 V to 1.0 V. The electrochemical measurements were performed in a Faraday cage.

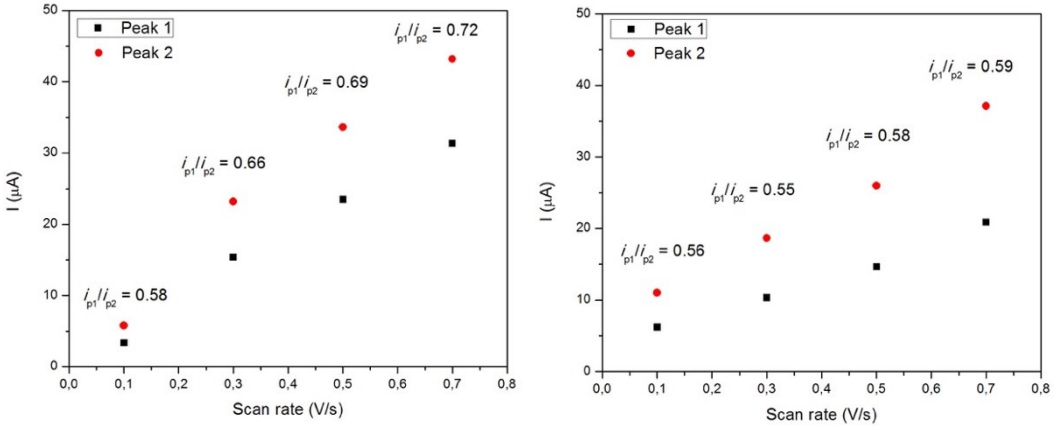

Figure S8. Dependence of the current versus scan rate of oxidation peaks p_{ox1} and p_{ox2} for SAMs **3** (left) and **4** (right) and ratio of the peak currents (i_{pox1}/i_{pox2}).

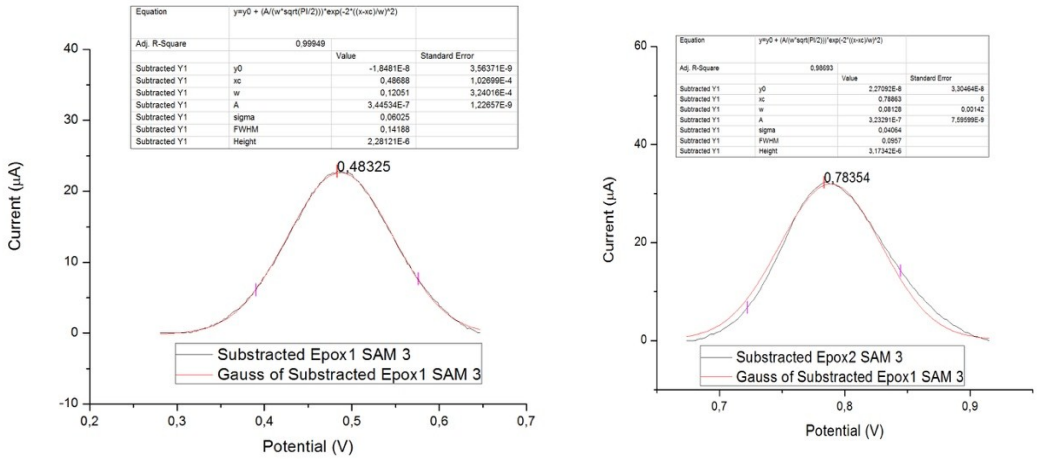

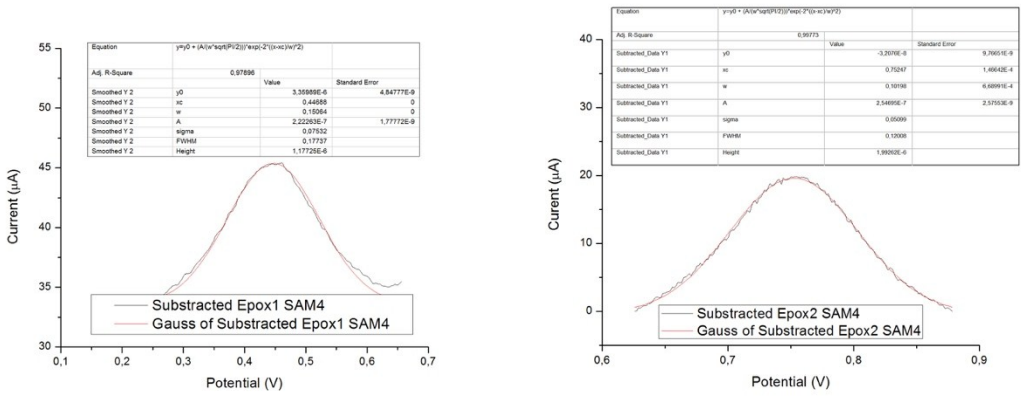

Figure S9. Subtracted CV peaks ($E_{1/2}^{ox1}$ and $E_{1/2}^{ox1}$) and fwhm values for SAMs **3** and **4**.

3.6. Photoelectron spectroscopy of PTM-TTF based SAMs 3 and 4

Synchrotron-based photoemission spectroscopy (PES) measurements (including X-ray and ultraviolet photoelectron spectroscopy) and near edge X-ray absorption fine structure (NEXAFS) spectroscopy were performed at the MBS (Materials Science Beamline) of Elettra Synchrotron (Trieste, Italy) and at the SINS (Surface, Interface and Nanostructure Science) beamline of Singapore Synchrotron Light Source (SSLS) which measurement and analysis procedures are reported elsewhere.[3] Briefly, the base pressure was kept at 1×10^{-10} mbar. We used the Au $4f_{7/2}$ core level peak at 84.0 eV measured from a sputter-cleaned gold foil in electrical contact with the sample to calibrate the photon energy. We chose 350 eV to probe the Cl 2*p*, S 2*p* and C 1*s*, and 60 eV for the valence band measurements. The work function was measured using 60 eV photon energy and we applied –10 V bias to the sample to overcome the work function of the analyzer. All UPS spectra were referenced to the Fermi edge of Au and all PES spectra were normalized by the photon current. The top of the valence band (HOMO onset) and work function (secondary electron cut-off) values were determined by linear extrapolation of the lower binding energy side of the HOMO peak and secondary electron cut-off intercepted with the linear extrapolation of the base line as denoted by the dotted lines and solid vertical bars in Figure S18b.[3] For NEXAFS, we measured the photon energy from 270 eV to 330 eV. Different take-off angles (90°, 60º and 30°) were used to probe the angle-dependence. We performed the least-square peak fit analysis with Voigt functions (Lorentzian (30%) and Gaussian (70%)) using XPSpeak software, and the sloping background was modelled using Shirley plus linear background correction.[4,5]

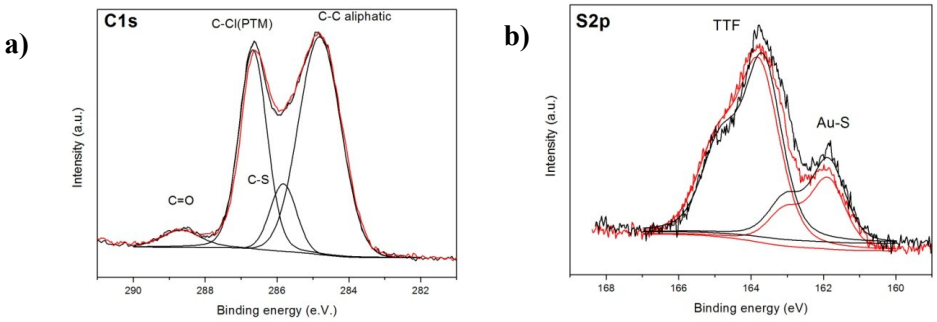

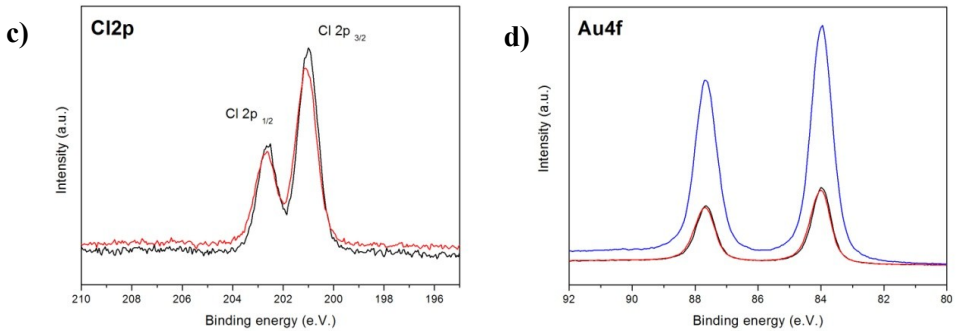

Figure S10. High resolution photoemission spectra of a) C1s b) S2p c) Cl2p and d) Au4f for SAMs of **3** (black line) and **4** (red line) measured at 500 eV. Blue line in Au4f is the blank (bare gold).

3.7. Thickness of PTM-TTF based SAMs 3 and 4

The film thicknesses of **SAMs** of **3** and **4** were also calculated from the high resolution PE spectra of Au_{4f} taken at 630 eV, shown in Figure S17, by evaluating the attenuation of the Au $4_{f7/2}$ peak of a sputtered substrate and for each functionalized substrate according to Equation 1 where I and I_o correspond to the substrate intensity of the SAM covered and bare surface, respectively; d is the SAM thickness, and θ is the detection angle with respect to the surface normal.

.

$$I = I_o \exp(-d/\lambda\cos\theta) \quad (1)$$

Here, $\theta = 0$, λ is the photoelectron attenuation length, and is characteristic of each system. λ depends on the kinetic energy of the photoelectrons and for these measurements it was assumed a value of 18.2 Å as reported for adenine[11] as model organic system, supported by the fact that similar values have been reported for organic systems. Results of thickness of **SAMs 3** and **4** are summarized in Table S1. The uncertainty of ±2 Å takes into account the fitting errors and the angular misalignment due to sample mounting.

Table S1. Calculated film thickness of **SAMs 3** and **4** on Au^{TS}.

SAMs	$I/I_{o\ Au\ 4f}$	d (nm)
SAM **3**	0.29	**2.1**
SAM **4**	0.20	**2.1**

3.8 UPS and NEXAFS of PTM-TTF based SAMs 3 and 4

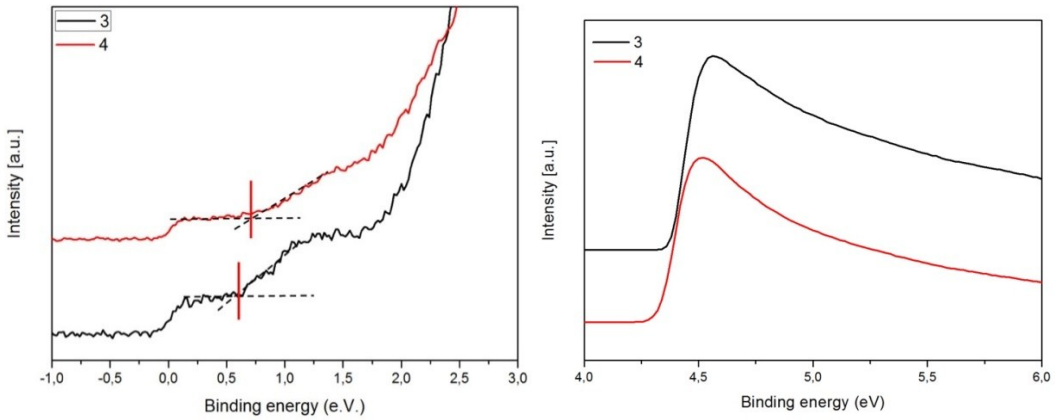

Figure S11. a) Valence band and b) secondary cut-off spectra of SAMs **3** (black line) and **4** (red line). The dashed lines in panel a show the procedure used to extract the value of the HOMO following the same procedures as reported previously.[3]

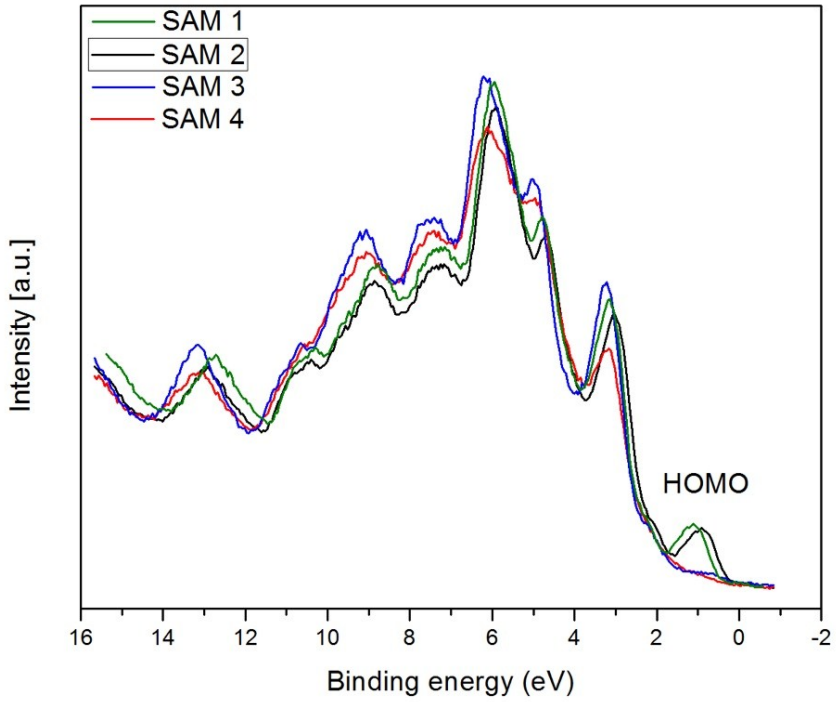

Figure S12. Valence band spectra of SAMs **1**-**4**.

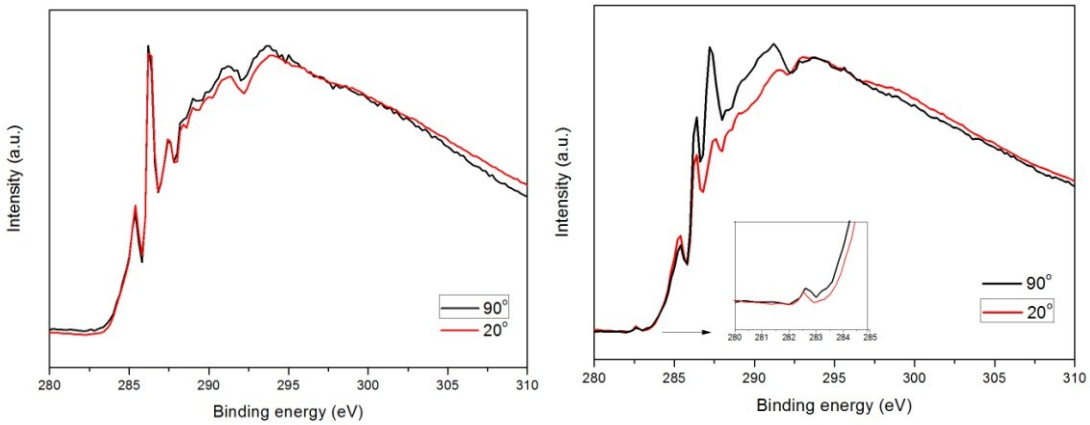

Figure S13. NEXAFS spectra of SAM **3** (left) and SAM **4** (right) in normal (NI, red line) and grazing (GI, black line) incidences. Inset shows the zoom in the 280-285 eV region.

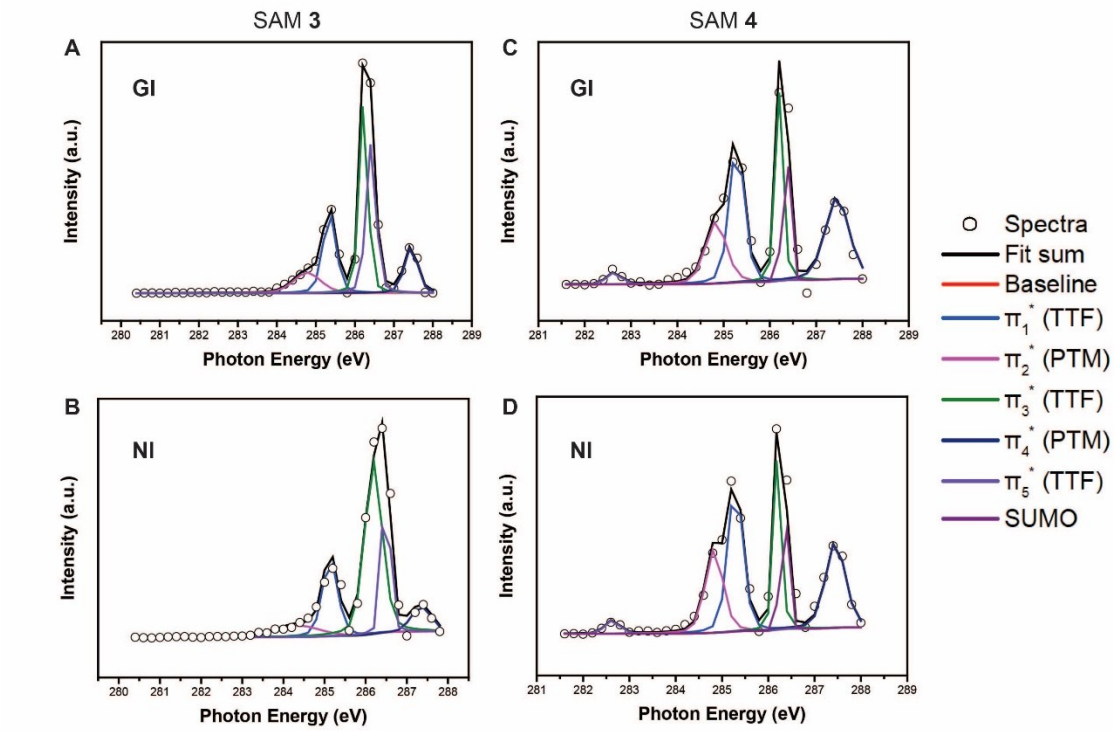

Figure S14. The fits to the NEXAFS spectra (with two different angles of incident light: 20º (GI) and 90º (NI)) of the SAMs **3** and **4**. The empty dots are the spectra and the solid lines are the background and fits.

3.8 Surface coverage of PTM-TTF based SAMs 3 and 4

To calculate the surface coverage of the SAMs derived from **3** and **4**, we determined the integrated intensity of Cl 2*p* spectra (I_{Cl}) of the SAMs (**3** and **4**) and $S(CH_2)_{10}CH_2Cl$ ($SC_{11}Cl$) SAMs (listed in the Table S2 below). Since the Cl atoms were connected to the terminal groups of the SAMs, the I_{Cl} can be related to the surface coverage of the SAMs. The relative surface coverage was calculated comparing the I_{Cl} of SAMs **3** and **4** (divided by 14 since SAMs **3** and **4** contain 14 Cl atoms) against that of $SC_{11}Cl$ SAMs. The surface coverage of $SC_{11}Cl$ SAMs on Ag surface has been reported before and is 1.1×10^{-9} mol/cm^2.[6] Thus, we compared the values of I_{Cl} of the SAMs **3** and **4** against that of $SC_{11}Cl$ SAMs to calculate the absolute surface coverage of the SAMs **3** and **4** (Table S2). We estimated the uncertainties are about 5% from the fitting errors of Cl 2*p* spectra. However, we notice that not all 14 Cl atoms of the PTM moiety were located at the top of the SAMs, and at least 4 Cl atoms (connected to the phenyl ring with alkyl chain) give lower signals due to attenuation by the other aromatic rings (or roughly half the length of the PTM moiety, ~6.3 Å) of the PTM moiety. Thus, the absolute surface coverage calculated by XPS here was underestimated by t at least 13% ($= {}^{4}/_{14} \times e^{-{}^{6.3}/_{\lambda}}$). Nevertheless, the relative surface coverages are for all the SAMs the same which supports our conclusion that we did not change the supramolecular structure of the SAMs. Surface coverages obtained by cyclic voltammetry were in the same range ($0.1\text{-}0.2 \times 10^{-9}$ mol/cm^2).

3.9 Calculation of tilt angles of TTF units in SAMs 3 and 4 from NEXAFS spectra

We fitted the NEXAFS spectra in the photon energy range from 284 to 291 eV with a Voigt function of Lorentzian (30%) and Gaussian (70%), and the fits to the spectra are shown in Supplementary fig. 22. We used the intensity (I) of π_3* to calculate the tilt angles (α) of TTF units. Assuming a random azimuthal orientation between molecules and substrate, the intensity ratio of π_3* resonances (I_{π^*}) at 90º and 20º incident angles can be expressed as follows:

$$\frac{I_{\pi^*}(\alpha,90°)}{I_{\pi^*}(\alpha,20°)} = \frac{P(\sin^2\alpha\sin^2 90° + 2\cos^2\alpha\cos^2 90°) + (1-P)\sin^2\alpha}{P(\sin^2\alpha\sin^2 20° + 2\cos^2\alpha\cos^2 20°) + (1-P)\sin^2\alpha} \quad (1)$$

in which $P = 0.90$ is the linear polarization factor of incident X-ray light.

Table S2. The values of I_{Cl}, relative surface coverage and absolute surface coverage.

SAMs	I_{Cl} at 90° take-off angle	Relative surface coverage[a]	Absolute surface coverage (× 10^{-9} mol/cm^2)
SAM **4**	39184	0.11	0.12
SAM **3**	42643	0.11	0.12
$SC_{11}Cl$	26450	1	1.10

[a] The relative surface coverage is calculated from $I_{Cl}(SC_{11}Cl)$ / (I_{Cl}(SAM **3** or **4**) / 14).

3.10 Calculation of LUMO energy levels from NEXAFS spectra of SAMs

We estimated the LUMO energy position (with respect to the vacuum level) from the first resonance peak of the NEXAFS spectra. In principle, the LUMO energy respected to the Fermi level is equal to the difference between the photon energy of the $4e_{1g}$ peak (PE_{LUMO}) and the C1s binding energy of cyclopentadienyl ring (BE_{Cp}). However, during the X-ray adsorption process, the electron is excited from the core level leaving behind a hole in the core level. This hole interacts with the electron in the excited state lowering the energy of the LUMO. The value of $BE_{exciton}$ is strongly dependent on the chemical formula of the molecule, the geometry of the molecule, the lattice structure and etc., and varies from 100 to 2000 meV.[7] Here we correct the estimated LUMO energy for this core-hole exciton binding energy

($BE_{exciton}$) using equation 2 and BEexciton = 500 meV taken from reference S10 which is typically used in thin organic films.

$$LUMO = PE_{LUMO} - BE_{Cp} + BE_{exciton} \quad (2)$$

3.11 Calculation of orbital energies from CV of SAMs

Information about the HOMO and LUMO energies of electroactive molecules grafted on an electrode, relative to vacuum, can be extracted from cyclic voltammograms using Equation 3; where $E_{abs,NHE}$ is the absolute potential energy of the normal hydrogen electrode (-4.5 eV), and $E_{1/2,NHE}$ is the formal half-wave potential of the grafted molecule *vs.* the normal hydrogen electrode (NHE).

$$E_{HOMO} = E_{abs,NHE} - eE_{1/2,NHE} \quad (3)$$

3.12 Fabrication of Au^{TS}-SAMs//GaO_x^{cond}/EGaIn junctions

The fabrication of the SAM-based junctions with cone-shaped tips of GaO_x^{cond}/EGaIn were reported previously.[8] Briefly, in our experiments we grounded the bottom electrode on which a gold probe penetrating the SAMs and the top-electrode of GaO_x/EGaIn was biased from 0V →1.0 V→ 0V →-1.0 V → 0V, with a step size of 50 mV, and a delay of 0.1 s, for the *J*(V) curve.

4 Computational details

4.1 SAMs 1-4

We have built a gold slab made of 5 gold layers and exposing the (111) surface by repeating a unit cell p (6x4√3) by periodic boundary conditions (PBC). The distances between the Au-Au were set at 2.88 Å, lattice parameters a=20.28 Å, b=17.45 Å, angle γ= 90º, yielding a surface area A=356.06 Å^2. For the highest degree of coverage (4 molecules per unit cell), the surface area per molecule is thus A=89.02 Å^2. The molecule and the repeating slab are separated in the third direction by a vacuum region of 35 Å in order to avoid electrostatic interactions between repeated units, whereas the dipole correction[9] was applied in this axis. Due to the high flexibility of the molecules, they are deposited on the surface in a frozen linear configuration previously optimized in geometry in the gas phase with constraints imposed to match the experimental layer thickness[10]. The sulfur atoms have been attached above Au (111) hollow site; no major influence of the anchoring site and number of sulfur atoms attached to Au is observed in the energy alignment (see Fig. S18).

The geometry optimizations of the isolated molecules were carried out by Density Functional Theory (DFT) calculations,[11] using the (Unrestricted) Perdew-Burke-Ernzerhof (U-PBE) exchange correlation functional[12] and a 6-31G(d) basis set,[13] as implemented in the Gaussian09 package[14]. In line with our previous theoretical investigations, [15-20] all calculations have been performed at the DFT level with the SIESTA 3.2 package, [21] within the Generalized Gradient Approximation (GGA), using the Perdew-Burke-Ernzerhof (PBE) exchange correlation functional.[12] The valence electrons are described within the Linear Combination of Atomic Orbitals (LCAO) approximation using a Double Zeta + Polarization (DZP) basis set[22] whereas Troullier-Martins pseudopotentials[23] are used for the description of the core electrons. Spin-polarization calculations were performed when dealing with the radical forms. We use a mesh cutoff of 250 Ry and a k-sampling[24] of (1,1,1) due to the large dimensions of the unit cell used to avoid interactions between the molecules at low degree of coverage.

4.2 Molecular junctions based on SAMs

Following the methodology used in previous works[25-29], the same molecular geometries used in the SAMs were connected to two semi-infinite parallel (111) Au surface electrodes, made of 3 layers (on the left side) and 4 layers (on the right side), with each layer made of 36 (6 × 6) Au atoms and PBC applied in the plane perpendicular to the transmission direction. Since a precise knowledge of the surface organization of the molecules in the SAM is missing, the unit cell has been chosen to match the size of the anchored molecules and to ensure weak interactions with molecules in the image cells (with distances larger than 10 Å). In all junctions, the chemisorbed sulfur atoms are anchored on a hollow site of the Au (111) surface, at a fixed distance of 2.4 Å. Moreover, despite XPS measurements show a mixing of molecules with one or two sulfur atoms attached to the gold substrate, for the sake of simplicity, we have considered only one sulfur attached; nevertheless, the energy alignment is similar with one versus two bounded sulfur(s) (see Figure 21) As the molecule is physisorbed on the top electrode contact , the distance between the highest Cl atom of the molecule and the gold atom of the surface has been fixed at 3.4 Å (equal to the sum of the van der Waals radii of Cl (1.75 Å) and Au (1.66 Å) atoms).

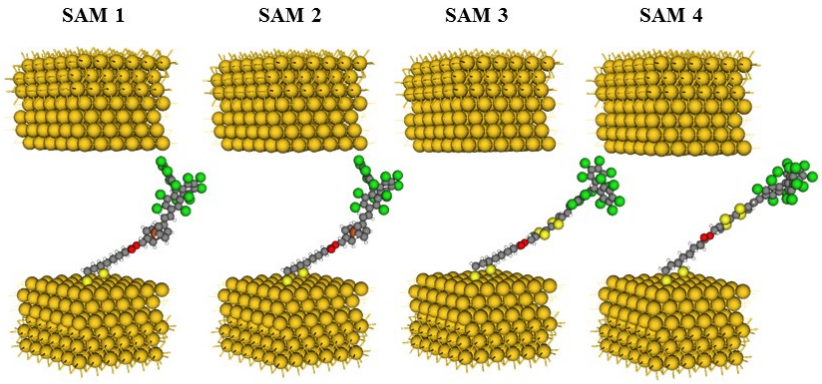

Figure S15. Structures of the unit cell of the molecular junction with **SAM 1** to **4** (from left to right).

The transmission spectra of the gold−molecule−gold junctions have been calculated using the widely used nonequilibrium Green's function (NEGF) formalism coupled to a DFT method, as implemented in the ATK2008.10 package.[30,31] The exchange correlation GGA.revPBE functional[12] has been used, with a SZP (DZP) basis set for valence Au electrons (the valence molecular orbitals), a (4 × 4 × 50) k-point sampling, a mesh cutoff of 180 Ry, and a temperature of 300 K. The core electrons are frozen and included in norm conserving Troullier−Martins pseudopotentials. The I/V characteristics have been calculated on the basis of Landauer formula[32] in a bias window between −2.0 and +2.0 V, with the bias step set to 0.4 eV.

5 Theoretical supporting results

5.1 Calculation of the degree of delocalization

As mentioned in the previous section, the program SIESTA relies on the Linear Combination of Atomic Orbitals (LCAO) approximation to describe the valence electrons. The wave function for a given a k-point (in our case Γ) ψ_i is expressed as a sum of the product of the atomic orbitals ϕ_i and LCAO coefficients c_i.

$$\psi_j = \sum_i^n c_{ij}\phi_i \tag{4}$$

Thus, the sum of the square of these coefficients c_i^2 for orbitals localized on a given atom reflects the contribution of that atom to the wave function. The delocalization of the molecular orbitals over the different parts of the molecules (Fc, PTM and vinylene bridge) can be expressed as:

$$r_{\psi,Fc} = \frac{\sum_{i}^{n_{Fc}} {c_{\psi,i}}^2}{\sum_{i}^{n_T} {c_{\psi,i}}^2}; \quad r_{\psi,TTF} = \frac{\sum_{i}^{n_{TTF}} {c_{\psi,i}}^2}{\sum_{i}^{n_T} {c_{\psi,i}}^2}; \tag{5 and 6}$$

$$r_{\psi,PTM} = \frac{\sum_{i}^{n_{PTM}} {c_{\psi,i}}^2}{\sum_{i}^{n_T} {c_{\psi,i}}^2}; \tag{7}$$

$$r_{\psi,bridge} = 1 - r_{\psi,Fc/TTF} - r_{\psi,PTM}; \tag{8}$$

with n_T the total number of atomic orbitals in the full system, n_{Fc} the number of atomic orbitals in the Fc unit and n_{PTM} the number of atomic orbitals in the PTM unit.

Table S3. Participation ratio of the different parts of the D-A dyads to the frontier MOs of SAM **1** and SAM **2** (top); SAM **3** and SAM **4** (bottom).

	SAM 1		**SAM 2**			
r_ψ	HOMO	LUMO	SOMO	HOMO	SUMO	LUMO
Fc	0.928	0.202	0.294	0.754	0.037	0.208
bridge	0.036	0.212	0.021	0.052	0.026	0.212
PTM	0.036	0.586	0.685	0.194	0.937	0.580

	SAM 3		**SAM 4**			
r_ψ	HOMO	LUMO	SOMO	HOMO	SUMO	LUMO
TTF	0.971	0.269	0.089	0.952	0.210	0.342
bridge	0.015	0.255	0.033	0.014	0.034	0.279
PTM	0.014	0.477	0.878	0.035	0.756	0.379

5.2 Supporting theoretical graphs and figures

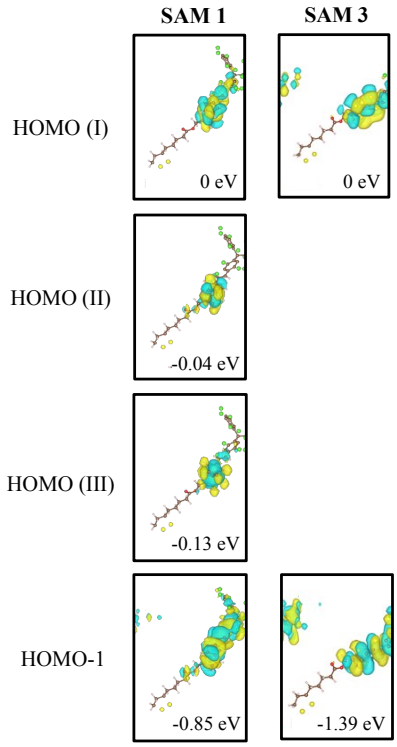

Figure S16. Shape of the frontier occupied orbitals for the closed-shell molecules **S1** (left) and **S3** (right). The inset numbers represent the relative energies with respect to the HOMO level. The isovalue used was 0.02 a.u.

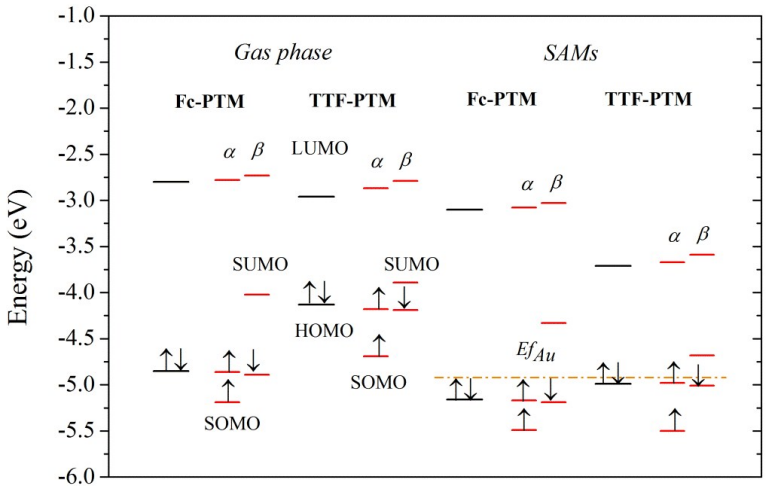

Figure S17. Energies of the frontier molecular orbitals for SAMs **1**, **2**, **3** and **4** (from left to right) molecules in the isolated state (left part) and corresponding orbitals upon adsorption on gold (right part). In this case we consider the lowest coverage (θ=0.25). The two lines for the radicals represent the spin up (α) and spin down (β) contributions. Only the orbitals localized over the Fc and/or PTM parts are reported here. The energies of the frontier molecular orbitals and the Fermi level of gold have been aligned with respect to the vacuum level[33]. The lowest coverage has been obtained by leaving in the same unit cell only one molecule out of the four molecules present at the highest coverage.

Table S4. Calculated Bader charges[34] for the studied SAMs adsorbed on Au as in Figure S17.

$\sum Q$	SAM **1**	SAM **2**	SAM **3**	SAM **4**
PTM	-0.136	-0.163	-0.106	-0.207
bridge	0.141	0.032	0.094	0.116
Fc/TTF	-0.001	0.184	0.002	0.123
alkyl	0.076	0.027	0.17	-0.046
DS	0.105	0.109	0.037	0.03
Au slab	-0.186	-0.189	-0.197	-0.215

The Bader charge analysis showed similar values of charge transfer between molecule and Au slab, thus veryfing that the interfacial charge transfer is not playing a big role in the relative alignment of the different SAMs.

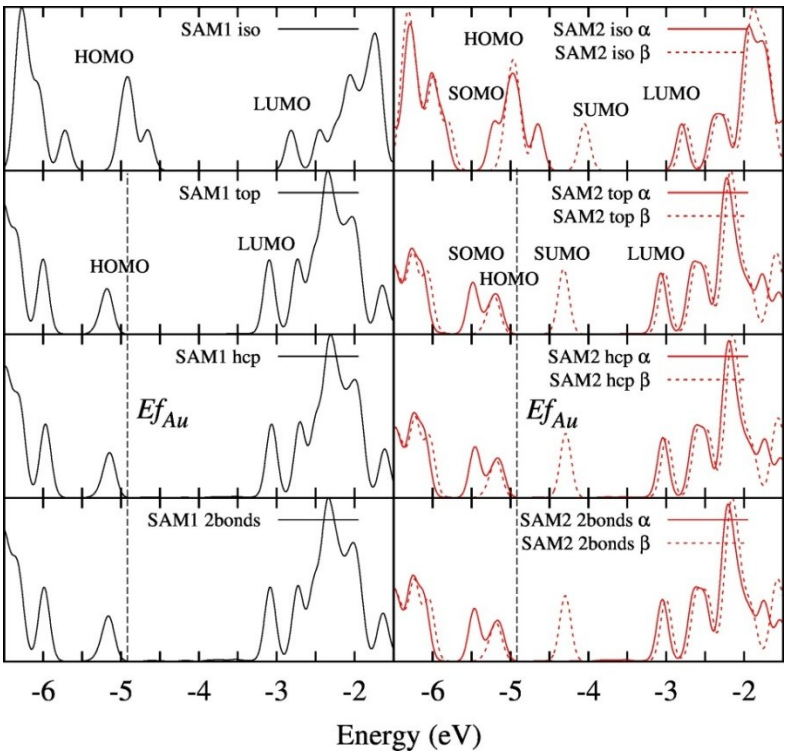

Figure S18. Density of States (DOS) of SAM **1** (black) and **2** (red) for the isolated molecules (iso) on the top and the molecules attached to Au: top (one S attached to one Au atoms), hollow (one S attached to three Au atoms) and two S bonded positions (one top and other hollow) respectively. Note that there are no big changes in the energy alignment due to the anchoring geometry.

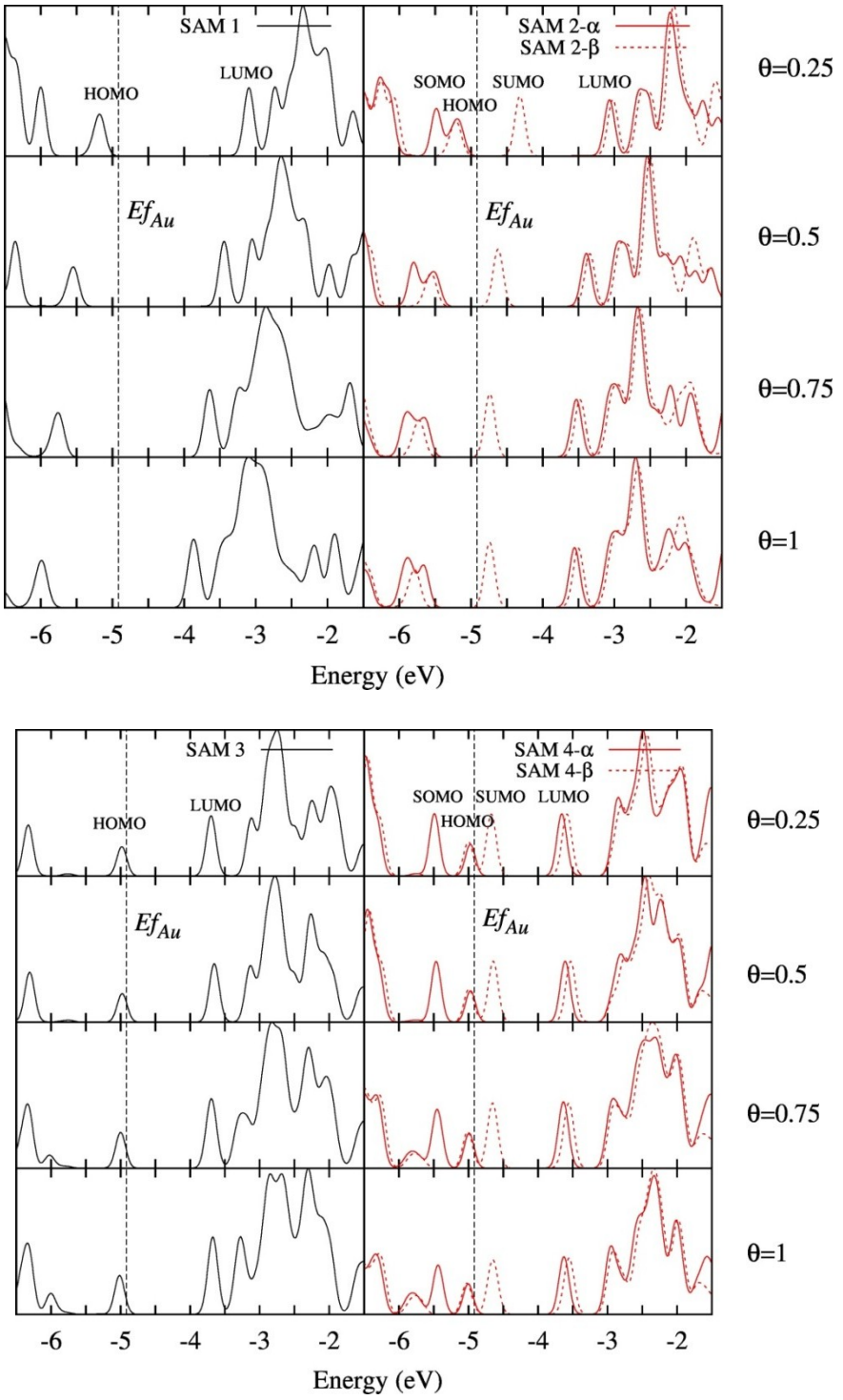

Figure S19. Density of States (DOS) of the SAMs **1** (top left), **2** (top right) **3** (bottom left) and **4** (bottom right) as a function of the degree of coverage: from θ=0.25 (top) to θ=1 (bottom).

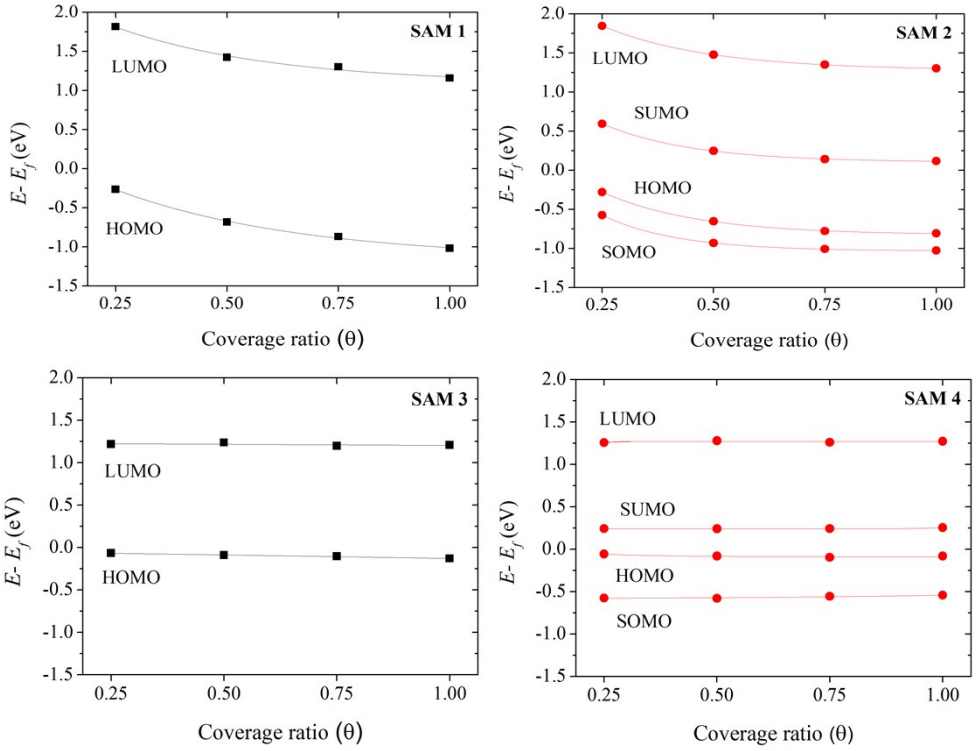

Figure S20. Frontier MO energy offsets of the SAMs **1** (top left), **2** (top right) **3** (bottom left) and **4** (bottom right) as a function of the degree of coverage: from θ=0.25 to θ=1. This evolution of the energy offsets with the coverage has been fitted with an exponential function $y=y_0+A*\exp(R_0*x)$.

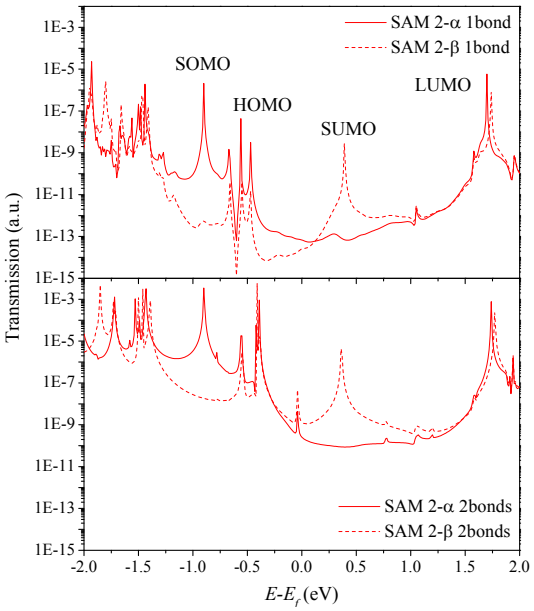

Figure S21. Transmission spectra at 0V for SAM **2** with one (top) and two (bottom) sulphurs attached to the Au slab. The dash and continuous lines of the right graph represent the spin up (α) and spin down (β) contributions, respectively.

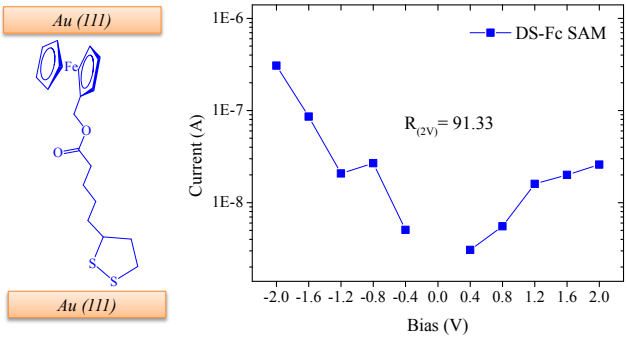

Figure S22. Chemical structure of the disulphide Fc (DS-Fc) SAMs (left) and calculated I-V curves for that SAMs.

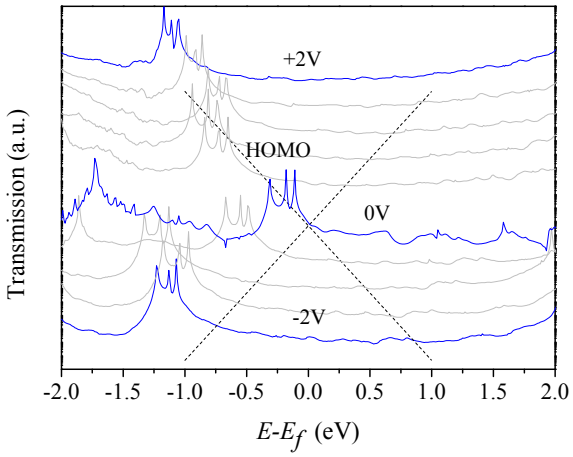

Figure S23. Evolution of the transmission spectra with bias (positive above and negative below) for the DS-Fc SAM. The bias step used was 0.4V.

6 References of the Supporting Information

(1) Rovira, C.; Ruiz-Molina, D.; Elsner, O.; Vidal-Gancedo, J.; Bonvoisin, J.; Launay, J. P.; Veciana, J. Influence of Topology on the Long-Range Electron-Transfer Phenomenon. *Chem. Eur. J.* **2001**, *7*, 240–250.

(2) Yuan, L.; Breuer, R.; Jiang, L.; Schmittel, M.; Nijhuis, C. A. A Molecular Diode with a Statistically Robust Rectification Ratio of Three Orders of Magnitude. *Nano Lett.* **2015**, *15*, 5506–5512.

(3) Yuan, L.; Nerngchamnong, N.; Cao, L.; Hamoudi, H.; del Barco, E.; Roemer, M.; Sriramula, R. K.; Thompson, D.; Nijhuis, C. a. Controlling the Direction of Rectification in a Molecular Diode. *Nat. Commun.* **2015**, *6*, 6324.

(4) Tour, J. M.; Jones, L.; Pearson, D. L.; Lamba, J. J. S.; Burgin, T. P.; Whitesides, G. M.; Allara, D. L.; Parikh, A. N.; Atre, S. Self-Assembled Monolayers and Multilayers of Conjugated Thiols, .alpha.,.omega.-Dithiols, and Thioacetyl-Containing Adsorbates. Understanding Attachments between Potential Molecular Wires and Gold Surfaces. *J. Am. Chem. Soc.* **1995**, *117*, 9529–9534.

(5) Ishida, T.; Choi, N.; Mizutani, W.; Tokumoto, H.; Kojima, I.; Azehara, H.; Hokari, H.; Akiba, U.; Fujihira, M. High-Resolution X-Ray Photoelectron Spectra of Organosulfur Monolayers on Au(111): S(2p) Spectral Dependence on Molecular Species. *Langmuir* **1999**, *15*, 6799–6806.

(6) Wang, D.; Fracasso, D.; Nurbawono, A.; Annadata, H. V.; Sangeeth, C. S. S.; Yuan, L.; Nijhuis, C. A. Tuning the Tunneling Rate and Dielectric Response of SAM-Based Junctions via a Single Polarizable Atom. *Adv. Mater.* **2015**, *27*, 6689–6695.

(7) Stohr, J. *NEXAFS Spectroscopy*; Springer.; Berlin, 1992.

(8) Nerngchamnong, N.; Yuan, L.; Qi, D.-C.; Li, J.; Thompson, D.; Nijhuis, C. a. The Role of van Der Waals Forces in the Performance of Molecular Diodes. *Nat. Nanotechnol.* **2013**, *8*, 113–118.

(9) Natan, A.; Kronik, L.; Shapira, Y. Computing surface dipoles and potentials of self-assembled monolayers from first principles. *Applied Surface Science* **2006,** 252, 7608–7613

(10) Souto, M.; Yuan, L.; Morales, D. C.; Jiang, L.; Ratera, I.; Nijhuis, C. A.; Veciana, J. Tuning the Rectification Ratio by Changing the Electronic Nature (Open-Shell and Closed-Shell) in Donor–Acceptor Self-Assembled Monolayers. *J. Am. Chem. Soc.* **2017**, *139*, 4262−4265.

(11) Kohn, W. Nobel Lecture: Electronic Structure of Matter—wave Functions and Density Functionals. *Rev. Mod. Phys.* **1971**, *71*, 1253–1266.

(12) Perdew, J. P.; Burke, K.; Ernzerhof, M. Generalized Gradient Approximation Made Simple. *Phys. Rev. Lett.* **1996**, *77*, 3865–3868.

(13) Rassolov, V. A. 6-31G* Basis Set for Third-Row Atoms. *J. Comput. Chem.* **2001**, *22*, 976–984.

(14) Frisch, M. J.; Trucks, G. W.; Schlegel, H. B.; Scuseria, G. E.; Robb, M. A.; Cheeseman, J. R.; Scalmani, G.; Barone, V.; Petersson, G. A.; Nakatsuji, H.; *et al.* Gaussian 09, Revision D.01. In *Gaussian Inc.*; Wallingford, CT, USA, **2013**.

(15) Crivillers, N.; Liscio A.; Di Stasio, F.; Van Dyck, C.; Osella, S.; Cornil, D.; Mian, S.; Lazzerini G.M.; Fenwick O.; Orgiu, E.; Reinders, F.; Braun, S.; Fahlman, M.; Mayor, M.; Cornil, J.; Palermo, V.; Cacialli, F.; Samorì, P. Photoinduced work function changes by isomerization of a densely packed azobenzene-based SAM on Au: a joint experimental and theoretical study. *Phys. Chem. Chem. Phys.* **2001**, *13*, 14302–14310.

(16) Crivillers, N.; Osella, S.; Van Dyck, C.; Lazzerini, G.M.; Cornil, D.; Liscio, A.; Di Stasio, F.; Mian, S.; Fenwick, O.; Reinders, F.; Neuburger, M.; Treossi, E.; Mayor, M.; Palermo, V.; Cacialli, F.; Cornil, J.; Samorì, P. Large work function shift of gold induced by a novel perfluorinated azobenzene-based self-assembled monolayer. *Adv. Mater.* **2013**, *25*, 432–436.

(17) Cornil, D.; Cornil, J. Work-function modification of the (111) gold surface upon deposition of self-assembled monolayers based on alkanethiol derivatives. *J. Electron Spectros. Relat. Phenomena.* **2013***, 189***,** 32–38.

(18) Cornil, D.; Li, H.; Wood, C.; Pourtois, G.; Prof. Brédas, J.-L.; Cornil, J. Work-function modification of Au and Ag surfaces upon deposition of self-assembled monolayers: Influence of the choice of the theoretical approach and the thiol decomposition scheme. *Chem. Phys. Chem.* **2013**, *14***,** 2939–2946.

(19) Osella, S.; Cornil, D.; Cornil, J. Work function modification of the (111) gold surface covered by long alkanethiol-based self-assembled monolayers. *Phys. Chem. Chem. Phys.* **2014***, 16***,** 2866–73.

(20) Fenwick, O.; Van Dyck, C.; Murugavel, K.; Cornil, D.; Reinders, F.; Haar, S.; Mayor, M.; Cornil, J.; Samorì, P. Modulating the charge injection in organic field-effect transistors: fluorinated oligophenyl self-assembled monolayers for high work function electrodes. *J. Mater. Chem. C,* **2015***, 3***,** 3007–3015.

(21) Sánchez-Portal, D.; Ordejón, P.; Artacho, E.; Soler, J. M. Density-functional method for very large systems with LCAO basis sets. *Int. J. Quantum Chem.* **1997**, *65***,** 453–461.

(22) Soler, J. M.; Artacho, E.; Gale, J.D.; García, A.; Junquera, J.; Ordejón, P.; Sánchez-Portal, D. The SIESTA method for ab initio order-N materials simulation. *J. Phys. Condens. Matter* **2002**, *14*, 2745.
(23) Troullier, N.; Martins, J. A straightforward method for generating soft transferable pseudopotentials. *Solid State Commun.* **1990**, *74*, 613–616.
(24) Pack, J. D.; Monkhorst, H. J. 'special points for Brillouin-zone integrations'-a reply. *Phys. Rev. B* **1997**, *16*, 1748–1749.
(25) Meng, F.; Hervault, Y.; Norel, L.; Costuas, K.; Van Dyck, C.; Geskin. V.; Cornil, J.; Hong. H.; Rigaut. S; Chen. X. Photo-modulable molecular transport junctions based on organometallic molecular wires. *Chem. Sci.* **2012**, *3*, 3113.
(26) Van Dyck. C.; Geskin V.; Kronemeijer, A. J.; de Leeuw, D.M.; Cornil J. Impact of derivatization on electron transmission through dithienylethene-based photoswitches in molecular junctions. *Phys. Chem. Chem. Phys*., **2013**, *15*, 4392-4404.
(27) Osella, S.; Samorì, P.; Cornil, J. Photoswitching Azobenzene Derivatives in Single Molecule Junctions: A Theoretical Insight into the I/V Characteristics. *J. Phys. Chem. C*, **2014**, *118*, 18721−18729.
(28) Osella, S.; Geskin, V., Cornil, J.; Beljonne, D. Coherent Electron Transmission across Nanographenes Tethered to Gold Electrodes: Influence of Linker Topology, Ribbon Width, and Length. *J. Phys. Chem. C*, **2014**, *118*, 7643−7652.
(29) Van Dyck, C.; Geskin, V.; Cornil, J. Fermi Level Pinning and Orbital Polarization Effects in Molecular Junctions: The Role of Metal Induced Gap States. *Adv. Funct. Mat.,* **2014**, *24*, 39.
(30) Taylor, J.; Guo, H.; Wang, J. Ab-Initio Modeling of Quantum Transport Properties of Molecular Electronic Devices. *Phys. Rev. B*, **2001**, *63*, 245407.
(31) Brandbyge, M.; Mozos, J.-L.; Ordejòn, P.; Taylor, J.; Stokbro, K. Density-Functional Method for Nonequilibrium Electron Transport. *Phys. Rev. B*, **2002**, *65*, 165401.
(32) Bütiker, M.; Imry, Y.; Landauer, R.; Pinhas, S. Generalized Many-Channel Conductance Formula with Application to Small Rings. *Phys. Rev. B*, **1985**, *31*, 6207−6215.
(33) Heimel, G.; Salzmann, I.; Duhm, S.; Koch, N. Design of Organic Semiconductors from Molecular Electrostatics. *Chem. Mater.*, **2011**, *23*, 359–377.
(34) Henkelman, G.; Arnaldsson, A.; Jónsson, H. A fast and robust algorithm for Bader decomposition of charge density. *Comput. Mater. Sci.* **2006**, *36,* 254-360.